

Imaging and histologic features of traumatic temporomandibular joint ankylosis

Jiang-Ming Li, MD,^a Jin-Gang An, MD,^a Xiao Wang, MD,^b Ying-Bin Yan, PhD,^c E. Xiao, PhD,^a Yang He, MD,^a and Yi Zhang, MD^a

Peking University, Beijing, China; Tianjin Stomatological Hospital, Tianjin, China

Objective. We aimed to study the pathology underlying traumatic temporomandibular joint ankylosis (TMJA).

Study Design. Specimens from 10 patients with traumatic TMJA were categorized using the Sawhney classification and were decalcified and stained with hematoxylin-eosin, alcian blue/periodic acid–Schiff, alizarin red, and Masson stains.

Immunostaining with anti-CD34 antibody was performed. Computed tomography and pathologic findings were compared.

Results. Ankylosed areas consisted of fibrocartilaginous tissues. Bone formation occurred by osteophyte extension from the osteochondral surface toward the mass center. Endochondral ossification and osteophyte proliferation, alone or simultaneously, participated in bony ankylosis. Sequestra in the cartilaginous ankylosis preferentially formed bony bridges. Newly formed capillaries participated in ossification from the bony surface of the bone-cartilage junction; bone formed around the capillaries. Osteoclasts were present at the capillary tips.

Conclusions. Types II and III were cartilaginous-bony ankylosis, with similar components. Bony traumatic TMJA was formed by osteophyte proliferation and endochondral ossification. (Oral Surg Oral Med Oral Pathol Oral Radiol 2014;118:330-337)

Temporomandibular joint ankylosis (TMJA) is the fibrous or bony union of the head of the mandibular condyle and the glenoid fossa.¹ The majority of TMJA cases are caused by trauma¹⁻⁷ (Table I). Sawhney⁸ proposed a 4-stage TMJA classification based on the clinical, imaging, operative, and gross pathologic findings in 70 patients. This classification is widely accepted. However, the computed tomography (CT) imaging and histologic characteristics of TMJA should be incorporated into the classification to improve the accuracy of the radiologic and histologic criteria of the classification. Some authors⁹⁻¹² have established animal models of TMJA, but the pathologic manifestations in these models are quite different from those in clinical patients. As different pathologic changes lead to different outcomes, the differences between the animal models and human patients are an important clinical concern. This article aims to describe in detail the CT and histologic characteristics of traumatic TMJA corresponding to the Sawhney classification. The information presented herein may be used as a basis for animal model establishment; furthermore, pathologic

evidence for the choice of clinical therapeutic method is provided by this study.

MATERIALS AND METHODS

Ten patients were enrolled in this study. All patients were men or boys who had been treated in the trauma center of Peking University School and Hospital of Stomatology (PUSHS) between July 2007 and February 2010 (Table II). Their mean age was 30.10 ± 12.72 years (range, 16-57 years), and all had a clear history of mandibular condyle fracture. No underlying comorbidities were detected. Their injuries had been caused by falls (5 patients), falls from a height (3 patients), and traffic accidents (2 patients). One patient had type I ankylosis, 5 had type II ankylosis, and 4 had type III ankylosis. The mean duration of the type I, II, and III ankylosis deformities was 6.00 ± 0.00 months, 91.20 ± 61.54 months, and 234.00 ± 108.00 months, respectively. We selected patients with types I, II, or III TMJA because during these stages, the ankylosis is not complete. This study was approved by the ethics committee of PUSHS (IRB00001052-11002); all patients provided written informed consent.

Panoramic radiographs and spiral CT scans in the coronal plane (Philips) were obtained. The following CT parameters were used: rotation time, 1 second; pitch, 1:1; slice thickness, 2 mm; voltage, 120 kV; maximum current,

This work was supported by the National Natural Science Foundation of China (Nos. 81070808 and 81170936).

^aDepartment of Oral and Maxillofacial Surgery, School and Hospital of Stomatology, Peking University.

^bDepartment of Stomatology, Peking University Third Hospital.

^cDepartment of Oral and Maxillofacial Surgery, Tianjin Stomatological Hospital.

Received for publication Dec 13, 2013; returned for revision May 5, 2014; accepted for publication May 7, 2014.

© 2014 Elsevier Inc. All rights reserved.

2212-4403/\$ - see front matter

<http://dx.doi.org/10.1016/j.oooo.2014.05.007>

Statement of Clinical Relevance

In this study, we correlate the CT findings in traumatic temporomandibular joint ankylosis, classified using Sawhney's classification approach, with the histopathologic changes.

Table I. The contribution of trauma in TMJA

Reference	Authors	Year published	Country	Traumatic	Total	%
1	Jain et al.	2008	India	40	44	90.90
2	El-Sheikh	1999	Egypt	201	204	98.50
3	Güven	2000	Turkey	27	42	64.82
4	Wen et al.	2002	China	32	42	74.20
5	Valentini et al.	2002	Italy	48	60	80.00
6	Ya et al.	2004	China	49	71	69.01
7	Elgazzar et al.	2010	Egypt	92	109	84.84

TMJA, temporomandibular joint ankylosis.

Table II. Distribution of the patients by TMJA type

Patient No.	TMJA type	Age (y)	Etiology	Side	Duration (mo)
1*	I	38	Traffic accident	Right	6
2	II	19	High fall	Right	144
3*	II	57	Fall	Right	48
4†	II	24	Fall	Right	96
5	II	17	High fall	Left	12
6	II	16	Fall	Right	156
7	III	30	Fall	Left	96
8*	III	36	Fall	Right	360
9	III	25	High fall	Double sides	240
10	III	39	Traffic accident	Left	240

TMJA, temporomandibular joint ankylosis.

No underlying comorbidities were detected. All patients were male.

*The slices from these patients were used as a model for types I, II, and III.

†The slices from the case in Figure 4.

130 mA; and automatic exposure control. Panoramic radiographs were used to determine the Sawhney⁸ type, and the accuracy of classification was verified using operative findings. The CT images corresponding to each Sawhney TMJA type were observed slice-by-slice and described in detail. The fusion line (FL) in the TMJA was detected on CT scans.¹³ The positions and characteristics of the FL were studied at focal points. The CT data were saved in DICOM (Digital Imaging and Communications in Medicine) format. Three-dimensional (3D) reconstructions of the CT images from patients with type I, type II, and III TMJA were prepared using SurgiCase software (Materialise Medical, Belgium; No. 8364-6D1F-8F2A-E56 B). The reconstructed images were separated along the FL. Segments of the fossae and condyles were observed and compared.

At surgery, the ankylosed mass was carefully exposed and harvested via the Al-kayat–Bramley incision, to protect the FL. The osteotomy planes were placed 5 mm above and 10 mm below the FL, and the lateral two-thirds of the bony mass was removed.

Histologic processing

All specimens were fixed in 10% buffered formalin for 24 hours and decalcified en bloc with 20% buffered ethylenediaminetetraacetic acid on a shaking table until

elastic deformation occurred. After being subjected to dehydration in a series of graded alcohols, the specimens were paraffin-embedded, cut into 4-µm-thick serial sections, and used for hematoxylin-eosin (HE), alcian blue/periodic acid–Schiff (AB-PAS), alizarin red (AR), and Masson staining as well as immunohistochemical staining with anti-CD34 antibody to identify neovessel formation. The antibodies were replaced with phosphate-buffered saline (PBS) in the case of a blank control, and a paraffin section of a human submandibular gland was used as a positive control. All sections were assessed using light microscopy.

HE staining and AB-PAS staining

The sections were deparaffinized and recombined for HE staining. For AB-PAS staining, in addition to these 2 steps, the sections were placed in distilled water, stained with 1% AB in 3% aqueous acetic acid (10-20 minutes), washed well in distilled water thrice (2 minutes each), treated with 1% periodic acid (5 minutes), stained with Schiff reagent (10 minutes), washed well in running tap water (10 minutes), dipped in 0.5% alum-hematoxylin solution (1-2 minutes), washed twice with tap water (10 seconds each), dipped in 1% ammonia solution (5-10 seconds), dehydrated, cleared, and mounted.

AR staining

The sections were deparaffinized, placed in distilled water, and stained with AR solution (0.5-5 minutes) until the red-orange staining indicating calcium was visible on microscopy. The excess stain was shaken off, and the sections were blotted, dehydrated, cleared, and mounted.

Masson staining

The sections were deparaffinized, placed in distilled water, stained with 0.5% hematoxylin (5-10 minutes), washed with tap water, dipped in a 1% hydrochloric acid–alcohol mixture (30-60 seconds), washed with tap water, dipped in 1:400 ammonia solution, washed well with tap water, stained with orange G (30-60 seconds), rapidly washed with tap water, stained with ponceau (4-5 minutes), dipped in distilled water (1-2 minutes), dipped in 1% phosphomolybdic acid (3-6 minutes), rapidly washed with distilled water, stained with bright green (10 minutes), washed with tap water, and mounted on a resinous mounting medium.

CD34 immunohistochemical staining

The sections were deparaffinized, placed in distilled water, washed with PBS, dipped in 3% H₂O₂ (10 minutes), washed with PBS (2 minutes), immersed

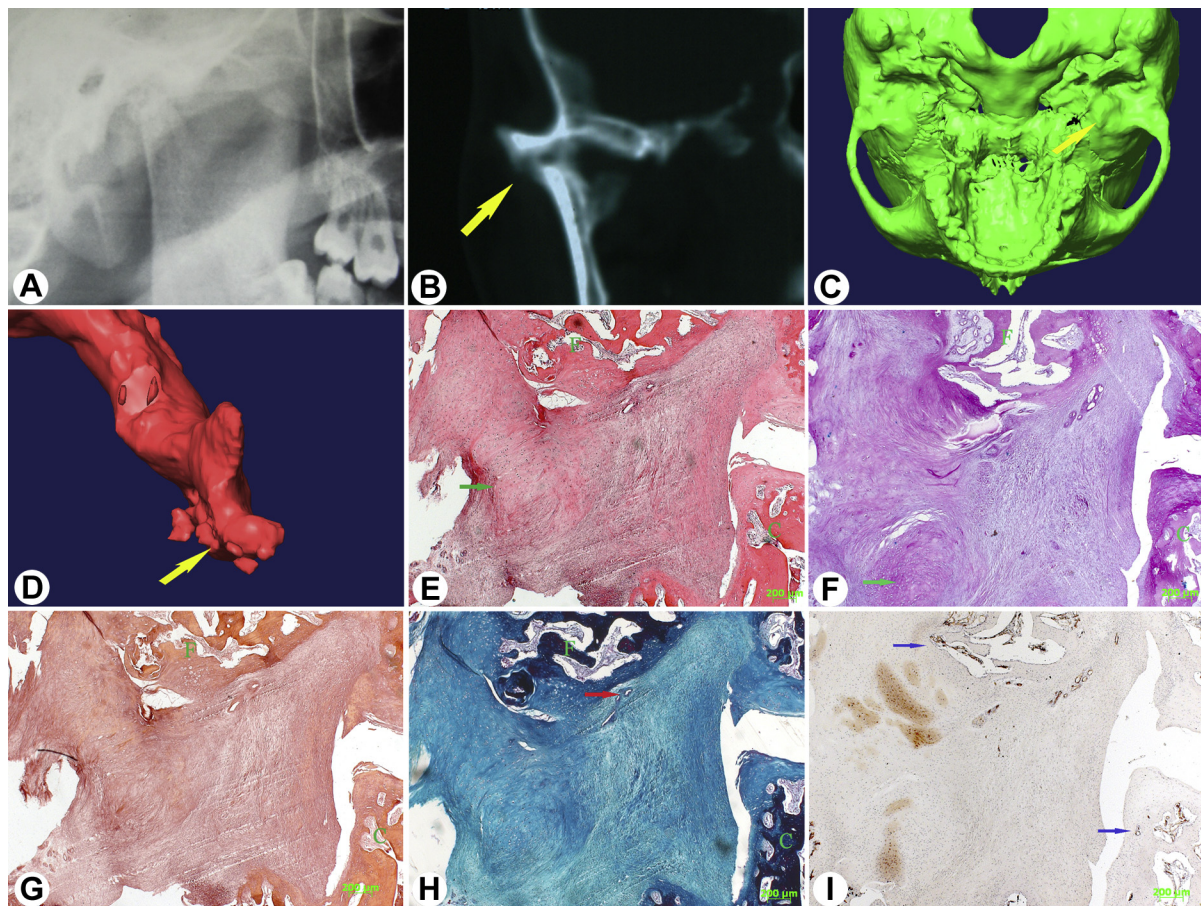


Fig. 1. Type I ankylosis. **A**, Panoramic radiograph of a right temporomandibular joint shows that the joint is still visible, but its borders are blurred. **B**, Coronal CT image shows that the joint is ankylosed, but the tissue (yellow arrow) connecting the fossa and condyle is hypocalcified. **C**, Three-dimensional CT reconstruction showing that the fossa (yellow arrow) has a smooth surface and normal anatomy. **D**, Three-dimensional CT reconstruction showing that the condyle (yellow arrow) is surrounded by some fragments. **E**, Hematoxylin-eosin staining shows newly formed hypertrophic chondrocytes (green arrow). **F**, Alcian blue/periodic acid-Schiff staining shows an island composed of hypertrophic chondrocytes (green arrow) and surrounded by fibrous tissue. **G**, Alizarin red staining shows different degrees of calcification in different tissues. Chondroid tissue is located between bony and fibrous tissue. **H**, Masson staining shows capillaries (red arrow) in a fibrous area. **I**, Immunohistochemical staining for CD34 antibody shows capillary walls (blue arrows) in the junction between the cartilaginous and bony ankylosed area. (F, fossa; C, condyle; CT, computed tomography. Original magnification for all images $\times 25$.)

in a water bath at 98°C (15 minutes), treated with 10% normal goat serum or PBS (blank control), and incubated at room temperature (30 minutes). The serum was discarded without rinsing the sections, and 1:100 CD34 class I antibody (ab8536, murine monoclonal antibodies; Abcam Company, Hong Kong) with PBS (or PBS only for blank controls) was dropped on the sections to distribute it. The sections were then incubated overnight at 4°C and washed 3 times with PBS (5 minutes each). A general-type immunoglobulin G-horseradish peroxidase polymer (PV-6002; Zhongshan Company, Beijing, China) was dropped on the sections, which were then incubated at 37°C (15 minutes) and rinsed twice with PBS (2 minutes each). Diaminobenzidine was added until satisfactory

coloration was obtained. The sections were then rinsed with tap water, dipped in 0.5% hematoxylin (3-5 minutes), doused in tap water (5 minutes), dehydrated, cleared, and mounted.

RESULTS

Type I ankylosis

Radiography. On panoramic radiographs, the condyle appeared flattened or deformed but closely approximated with the upper articular surface⁸ (Figure 1, A). On coronal CT images, flattening deformation of the condyle was confirmed, but the condyle could still be identified. Consistent with the panoramic radiography findings, the ankylosed condyle-fossa junction appeared blurred on CT, but the joint structure was distinct. In addition,

medial displacement of the fractured condyle was visible (see Figure 1, B). The outlines of the condyle and fossa were continuous and clear, and the surfaces of the condyle and fossa were almost smooth, except for some bony spurs visible on the 3D reconstructed images (see Figure 1, C).

Histology. HE staining showed that the mass in the joint space was composed of fibrous and cartilaginous tissue arranged in layers (see Figure 1, E). Massive hypertrophic chondrocytes were detected in the injured condylar area. The fossa and condyle were connected by chondroid tissue in some areas. The border between the fibrous and bony tissues was clear. Cartilaginous tissue was stained fuchsia by AB-PAS; however, the articular cartilage was hypochromatic, and the hypertrophic chondrocytes were unstained (see Figure 1, F). On AR staining, the border between the fibrous tissue and bone was much clearer than the one between the cartilaginous tissue and bone. Bone tissue was rarely observed in the connective tissue mass of the joint space. Scanty cartilaginous islands surrounded by fibrous tissues were observed occasionally (see Figure 1, G). On Masson staining, the FL area appeared brilliant green, which indicated cartilage or fibrous tissues; bone and calcified cartilage appeared red. Numerous capillaries were located in the fibrous area, but few were present in the cartilaginous area (see Figure 1, H). CD34⁺ cells were present in the cartilaginous area, the capillary wall in the fibrous ankylosed tissue, and the junction between the cartilaginous ankylosed tissue and bony segment, but not in the fibrous tissue (see Figure 1, I).

Type II ankylosis

Radiography. The panoramic radiography findings exactly matched the characteristics of type II TMJA according to the Sawhney classification.⁸ The condyle was misshapen or flattened but remained distinguishable and lay in close approximation with the fossa. However, bony fusion was established on the lateral edge of the articular surface, either anteriorly or posteriorly, but was limited to a small area (Figure 2, A). On coronal CT, bony fusion of the lateral portions of the fossa and condyle was confirmed, but in the medial part, the space between the cranial base and the residual condyle was intact, was well-demarcated, and resembled pseudarthrosis. The misshapen condyle was not flattened but thick in the coronal dimension (see Figure 2, B). The 3D reconstructed images showed that the condyle and fossa were irregular, shallow, or deep and sclerosed. The engagement of osteophytes from 2 surfaces resembled canine teeth. A concavity was present between the lateral part and the residual condyle (see Figure 2, C, D).

Histology. HE staining showed that the majority of the FL consisted of abundant fibrocartilaginous tissue. The finger-like osteophytes extended toward the articular surface contralateral to the injured area from the junction between the cartilaginous ankylosis and the bony surface. This finding was consistent with that observed on 3D CT reconstructions. Capillaries were present in the junction between the cartilaginous ankylosis and the bony surface and in the osteophyte centers (see Figure 2, E). The cartilaginous ankylosed area appeared a deep reddish purple on AB-PAS staining (see Figure 2, F) but hypochromatic on AR staining (see Figure 2, G). The entire FL appeared bright green on Masson staining, and the borders were clear (see Figure 2, H). The capillary walls in the junction of the cartilage and bony ankylosed area and in the junction of the sequestrum and marrow cavity were CD34⁺ (see Figure 2, I).

Type III ankylosis

Radiography. Panoramic radiography showed a bone bridge across the ramus of the zygomatic arch, which is consistent with the description of type III TMJA in the Sawhney classification (Figure 3, A). However, on coronal CT images, the fossa-condyle mass showed massive expansion, completely obscuring the joint structure. The FL was still visible but more blurred than that in type II TMJA. The joint space had disappeared in some areas (see Figure 3, B). Ankylosed bone was present throughout the joint, and bony fusion was present in the lateral part. The fossa-condyle junction and osteophytes were identical to those in type II, but the concavity in the condyle was indistinct (see Figure 3, C, D).

Histology. The results were similar to those for type II TMJA. Cartilaginous-bony ankylosis was seen (see Figure 3, E). Sequestra were cores of the bony bridges. The FL was present, but much narrower than that in type II TMJA. AB-PAS and AR staining showed that the FL was composed of mucopolysaccharide and was hypocalcified. The mucopolysaccharide in the cartilaginous ankylosis area still existed when the bony ankylosis had been established, whereas collagens in the FL or bony area were difficult to distinguish on Masson staining (see Figure 3, F-H). The sequestrum was surrounded by newly formed bone and CD34⁺ cells (see Figure 3, I).

DISCUSSION

Panoramic radiographs, coronal CT scans, and the results of pathologic examinations in patients with types I, II, and III TMJA were studied. We confirmed that most of the descriptions of these 3 types in the Sawhney⁸ classification are accurate. Sawhney⁸ considered

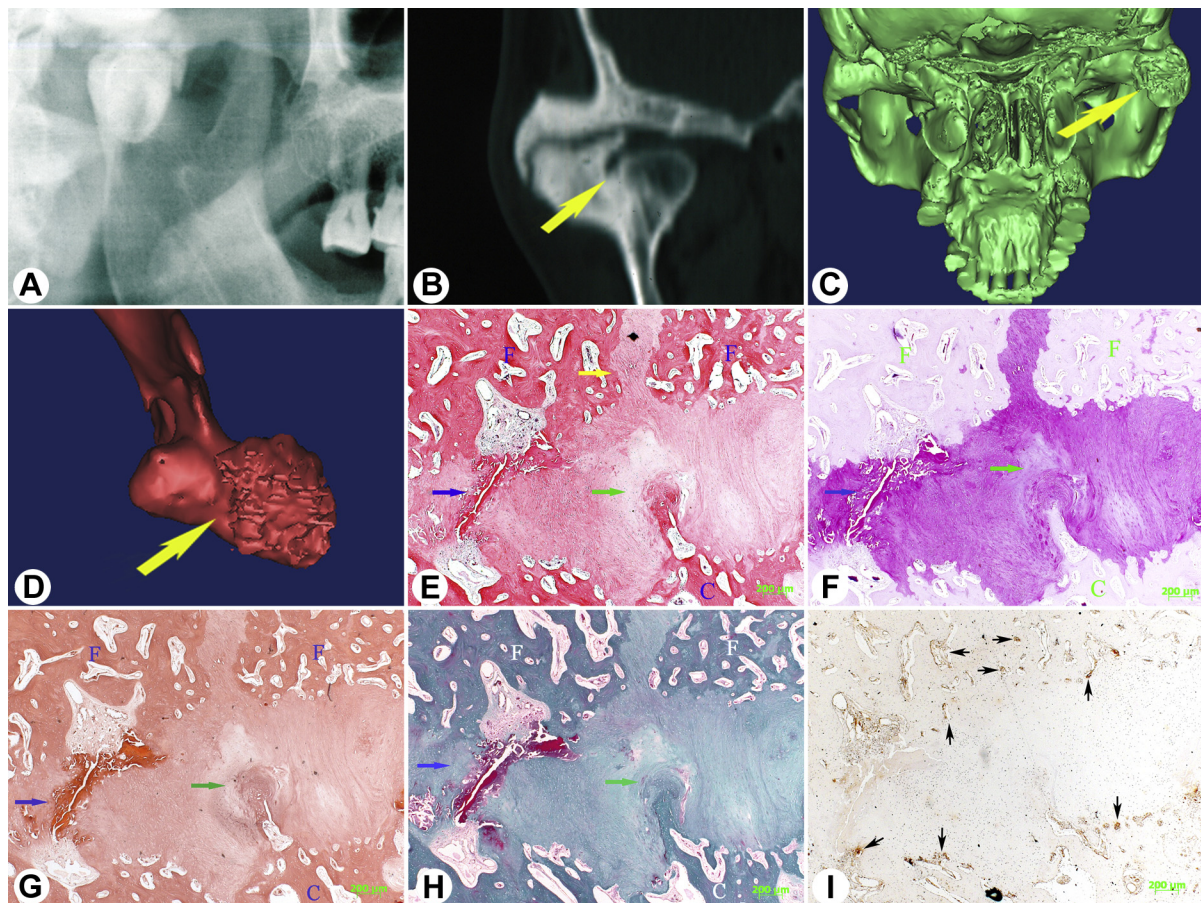


Fig. 2. Type II ankylosis. **A**, Panoramic radiograph shows that the anterior part of the joint is ankylosed. The joint space has disappeared in some parts. **B**, Coronal CT image shows that the lateral ankylosed area and the medial pseudarthrosis are separated by a depression (yellow arrow). **C**, Three-dimensional CT reconstruction shows that the fossa (yellow arrow) has a clear, smooth surface in the medial part and a normal, undamaged shape. **D**, Three-dimensional CT reconstruction showing that the condyle has fusion areas (yellow arrow) in the lateral part. Hematoxylin-eosin (**E**), alcian blue/periodic acid–Schiff (**F**), alizarin red (**G**), and Masson staining (**H**) show a bony bridge (blue arrows) composed of a sequesterum connecting with the bony surface of the condylar segment. A newly formed osteophyte (green arrow) extends from the condylar surface toward the fracture area on the surface of the fossa. Analysis of panels **E–H** suggests the following: (1) The newly formed osteophyte originated from the cartilage, as mucopolysaccharide is detected in its tip (**F**), which shows a low level of calcification (**G**). (2) The components in the fracture area of the fossa and the fusion line are the same, implying that the ankylosed process is similar to the fracture healing process (yellow arrow, **E**). (3) The sequesterum in the fusion line connecting the fossa and the condyle with a bony bridge (blue arrow, **G**) has a high level of calcification and was formed earlier than the osteophyte. (4) The osteophyte grows toward the fracture area of the fossa, that is, the trauma to the fossa contributes to ankylosis formation. **I**, Immunohistochemical staining shows that the capillary walls (black arrows) in the junction of the cartilage and bony ankylosed area and in the junction of the sequesterum and marrow cavity are CD34⁺. (F, fossa; C, condyle; CT, computed tomography. Original magnification for all images × 25.)

that type I ankylosis was fibrous. Yan et al¹² suggested that fibrous and fibrous-bony ankylosis types were caused by different pathologic processes. We confirmed that types II and III ankylosis appear fused on radiographs but show FLs on CT. Histologic studies also showed that the FLs in these types consist of fibrous, cartilaginous, and bony tissues. Types II and III ankylosis consisted of cartilaginous-bony tissues but differed in terms of the size of the ankylosed mass and functional changes.¹³ The difference between types II and III TMJA was in the size of the ankylosed mass not

only in the sagittal dimension (as Sawhney⁸ described) but also in the coronal and vertical dimensions. Another difference was the presence of the concavity in the bifid mandibular condyle, which was difficult to detect on panoramic radiographs. Hypertrophic chondrocytes were present near the bone-cartilage junction at the FL in all 3 types of TMJA, indicating early endochondral ossification. In all TMJA types, pathologic evidence of ossification was present at the junction between the FL and the bone, implying that ossification mainly occurred in the cartilaginous area. Enhanced CT in the

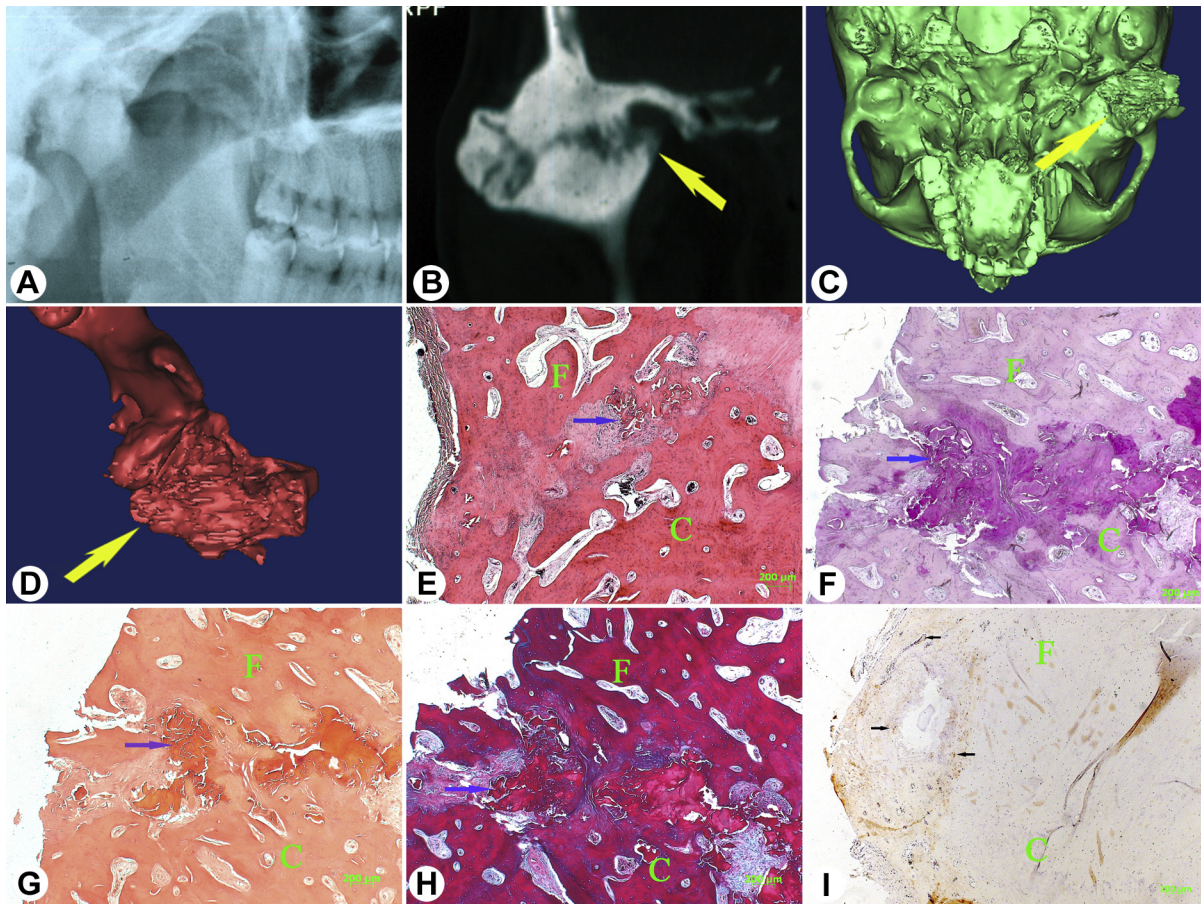


Fig. 3. Type III ankylosis. **A**, Panoramic radiograph showing that the whole joint has become a bony mass, but the joint space is still visible in the posterior part. **B**, Coronal CT shows that the internal pseudarthrosis has been replaced by a bony mass (yellow arrow). Ankylosis also affects the internal part of the joint. Three-dimensional CT reconstructions show that (**C**) the surface of the fossa (yellow arrow) has been totally damaged, and that osteophytes extend outward from the surface of the fossa and (**D**) the condyle (yellow arrow). The boundary between the fusion area in the lateral part and the internal residual condyle has disappeared. Hematoxylin-eosin (**E**), alcian blue/periodic acid–Schiff (**F**), alizarin red (**G**), and Masson staining (**H**) show that the bony mass is composed of newly formed bone and sequestra, but the fusion line can still be detected in some areas. Bony bridges are mainly formed by the sequestra (blue arrows). **I**, Immunohistochemical staining for anti-CD34 antibody shows that the sequestrum is surrounded by capillary walls (black arrows). (*F*, fossa; *C*, condyle; *CT*, computed tomography. Original magnification for all images $\times 25$.)

coronal plane is considered to be the best examination to avoid image superimposition during TMJA evaluation.¹⁴ However, we consider that plain coronal CT images clearly show the internal structure of the ankylosed mass. The direction of hyperostosis was from one bony surface to the impingement on the contralateral facies ossea, and this characteristic could be depicted more intuitively on reconstructed CT images.

Angiogenesis occurs early during endochondral and intramembranous osteogenesis.¹⁵ Traumatic TMJA involves osteogenesis, which can be disturbed by blocking angiogenesis^{16,17} and accelerated by stimulating angiogenesis.^{18,19} CD34 is selectively expressed in hematopoietic progenitor cells in the bone marrow and in endothelial cells in many nonhematopoietic

organs,^{20,21} but not in peripheral blood cells,²² and can therefore be used for the identification of newly formed capillaries.^{23,24} In the postnatal period, new capillaries develop from the congenital vasculature and endotheliocytes in peripheral circulation.^{25,26} CD34 may be expressed in endotheliocytes during vasculogenesis, so it can be used as a marker for endothelial abluminal microprocesses during angiogenesis.²⁷ CD34⁺ cells in the cartilaginous ankylosed area may be endotheliocytes with the potential to form new capillaries. These cells secrete several angiogenetic factors, including vascular endothelial growth factor, hepatocyte growth factor, and insulin-like growth factor 1,²⁸ which could accelerate angiogenesis. Furthermore, CD34⁺ cells also have the potential to differentiate into osteoblasts.²⁹ As CD34⁺ cells were detected only on the boundary of the

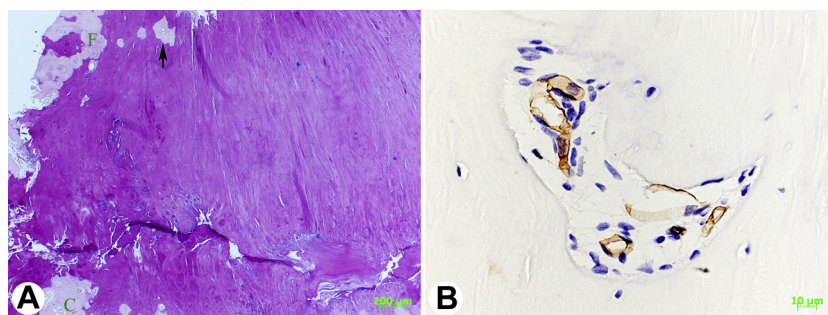


Fig. 4. The bone islands in Type II ankylosis. Islands of newly formed bone are detected near the cartilage-bone junction. The border between the bone islands and cartilaginous tissues appears distinct. The center of the bone island (black arrow) is composed of new capillaries (original magnification $\times 25$) and $CD34^+$ vascular endothelial cells (original magnification $\times 400$). **A**, Alcian blue/periodic acid-Schiff staining. **B**, Immunohistochemical staining of the island marked by the black arrow in panel A. (F, fossa; C, condyle.)

FL, and as AR staining demonstrated a difference between the FL and bone, we considered that angiogenesis and calcification occurred along the cartilaginous-bony junction, which played a major role in the formation of bony TMJA.

Sequestra are the outcomes of fracture fragments suspended in a hematoma after joint destruction. In all slices from type II and III specimens, sequestra were located in the cartilaginous ankylosed area, where bony bridges were first established. Osteoclasts were only present in sequestra that had fused with osteophytes. New capillaries were found in the fused areas on immunohistochemical staining. Living bony islands were not detected in the center of the FL (Figure 4). We hypothesized that fracture fragments in the fibrous ankylosed area would be absorbed by osteoclasts because this area has a good blood supply, whereas fragments in the cartilaginous area would be maintained because of a poor blood supply. Another hypothesis is that cartilage formation in the ankylosed area is stimulated by the sequestra, whereas hematomas not containing sequestra are transformed to fibrous ankylosed tissue. Future research should attempt to determine whether sequestra facilitate osteophyte formation or whether some other mechanism is involved.

In this study, specimen decalcification was a lengthy process, and the higher the classification type of the specimen, the more time was needed for decalcification. This may explain why the histochemical staining were not uniformly satisfactory. A more efficient neutral decalcification method needs to be found. Type IV ankylosis was not included in this study, as the FL disappears at this stage.

CONCLUSION

The Sawhney classification can generally reveal the severity of TMJA, but CT imaging is essential to improve preoperative evaluation. CT findings are more

consistent with the histologic results. Type I ankylosis is mild in terms of the size and severity of the ossification of the FL. Types II and III are more severe and consist of a cartilaginous-bony tissue ankylosed mass. Osteogenesis occurs in the junction between the cartilaginous ankylosed tissue and the bony segment mainly by endochondral ossification.

We thank Prof Yan Chen of the Pathology Department and Deng-Cheng Wu of the Central Laboratory of the School and Hospital of Stomatology, Peking University, for their assistance.

REFERENCES

- Jain G, Kumar S, Rana AS, Bansal V, Sharma P, Vikram A. Temporomandibular joint ankylosis: a review of 44 cases. *Oral Maxillofac Surg*. 2008;12:61-66.
- El-Sheikh MM. Temporomandibular joint ankylosis: the Egyptian experience. *Ann R Coll Surg Engl*. 1999;81:12-18.
- Güven O. A clinical study on temporomandibular joint ankylosis. *Auris Nasus Larynx*. 2000;27:27-33.
- Wen JQ, Jian XC, Tang ZG, Guo F. Etiological analysis of temporomandibular joint ankylosis. *J Mod Stomatol (chin)*. 2002;16:565.
- Valentini V, Vetrano S, Aqrillo A, Torroni A, Fabiani F, Iannetti S. Surgical treatment of TMJ ankylosis: our experience (60 cases). *J Craniofac Surg*. 2002;13:59-67.
- Ya ZM, Tan YH, Wang JM, Zhang G, Li ZY. Titanium condyle prosthesis for the treatment of temporomandibular joint ankylosis—71 cases report. *J Plast Reconstr Surg*. 2004;1:74-77.
- Elgazzar RF, Abdelhady AI, Saad KA, et al. Treatment modalities of TMJ ankylosis: experience in Delta Nile, Egypt. *Int J Oral Maxillofac Surg*. 2010;39:333-342.
- Sawhney CP. Bony ankylosis of the temporomandibular joint: follow-up of 70 patients treated with arthroplasty and acrylic space interposition. *Plast Reconstr Surg*. 1986;77:29-40.
- Miyamoto H, Kurita K, Ishimaru J, Goss AN. A sheep model for temporomandibular joint ankylosis. *J Oral Maxillofac Surg*. 1999;57:812-817.
- Miyamoto H, Kurita K, Ogi N, Ishimaru J, Goss AN. The effect of an intra-articular bone fragment in the genesis of temporomandibular joint ankylosis. *Int J Oral Maxillofac Surg*. 2000;29:290-295.

11. Cheunk LK, Shi XJ, Zheng LW. Surgical induction of temporomandibular joint ankylosis: an animal model. *J Oral Maxillofac Surg.* 2007;65:993-1004.
12. Yan YB, Zhang Y, Gan YH, An JG, Li JM, Xiao E. Surgical induction of TMJ bony ankylosis in growing sheep and the role of injury severity of the glenoid fossa on the development of bony ankylosis. *J Craniomaxillofac Surg.* 2013;41:476-486.
13. Yan YB, Zhang Y, Gan YH, Sun ZP, Li JM, Xiao E. The relationship between mouth opening and computed tomographic features of posttraumatic bony ankylosis of the temporomandibular joint. *Oral Surg Oral Med Oral Pathol Oral Radiol Endod.* 2011;111:354-361.
14. El-Hakim IE, Metwalli SA. Imaging of temporomandibular joint ankylosis: a new radiographic classification. *Dentomaxillofac Radiol.* 2002;31:19-23.
15. Kanczler JM, Oreffo RO. Osteogenesis and angiogenesis: the potential for engineering bone. *Eur Cell Mater.* 2008;15:100-114.
16. Hausman MR, Schaffler MB, Majeska RJ. Prevention of fracture healing in rats by an inhibitor of angiogenesis. *Bone.* 2001;29:560-564.
17. Gaston MS, Simpson AH. Inhibition of fracture healing. *J Bone Joint Surg Br.* 2007;89:1553-1560.
18. Eckardt H, Ding M, Lind M, Hansen ES, Christensen KS, Hvid I. Recombinant human vascular endothelial growth factor enhance bone healing in an experimental nonunion model. *J Bone Joint Surg Br.* 2005;87:1434-1438.
19. Li R, Stewart DJ, von Schroeder HP, Mackinnon ES, Schemitsch EH. Effect of cell-based VEGF gene therapy on healing of a segmental bone defect. *J Orthop Res.* 2009;27:8-14.
20. Watt SM, Karhi K, Gatter K, et al. Distribution and epitope analysis of the cell membrane glycoprotein (HPCA-1) associated with human hemopoietic progenitor cells. *Leukemia.* 1987;1:417-426.
21. Beschorner WE, Civin CI, Strauss LC. Localization of hematopoietic progenitor cells in tissue with the anti-My-10 monoclonal antibody. *Am J Pathol.* 1985;119:1-4.
22. Civin CI, Strauss LC, Brovall C, Fackler MJ, Schwartz JF, Shaper JH. Antigenic analysis of hematopoiesis. III. A hematopoietic progenitor cell surface antigen defined by a monoclonal antibody raised against KG-1a cells. *J Immunol.* 1984;133:157-165.
23. Bettencourt MC, Bauer JJ, Sesterhenn IA, Connelly RR, Moul JW. CD34 immunohistochemical assessment as a prognostic marker for prostate cancer recurrence after radical prostatectomy. *J Urol.* 1998;160:459-465.
24. Kim HS, Kang HS, Messam CA, Min KW, Park CS. Comparative evaluation of angiogenesis in gastric adenocarcinoma by nestin and CD34. *Appl Immunohistochem Mol Morphol.* 2002;10:121-127.
25. Asahara T, Murohare T, Sullivan A, et al. Isolation of putative progenitor endothelial cells for angiogenesis. *Science.* 1997;275:964-967.
26. Asahara T, Murohare T, Takahashi T, et al. Bone marrow origin of endothelial progenitor cells responsible for postnatal vasculogenesis in physiological and pathological revascularization. *Circ Res.* 1999;85:221-228.
27. Schlingemann RO, Rietveld FJ, de Woual RM, et al. Leukocyte antigen CD34 is expressed by a subset of cultured endothelial cells and on endothelial abluminal microprocesses in the tumor stroma. *Lab Invest.* 1990;62:690-696.
28. Majka M, Janowska-Wieczorek A, Ratajczak J, et al. Numerous growth factors, cytokines, and chemokines are secreted by human CD34(+) cells, myeloblasts, erythroblasts, and megakaryoblasts and regulate normal hematopoiesis in an autocrine/paracrine manner. *Blood.* 2001;97:3075-3085.
29. Tomoyuki M, Ryosuke K, Yutaka M, et al. Circulating endothelial/skeletal progenitor cells for bone regeneration and healing. *Bone.* 2008;43:434-439.

Reprint requests:

Yi Zhang, MD
Department of Oral and Maxillofacial Surgery
School and Hospital of Stomatology
Peking University
22 Zhongguancun Nandajie St
Beijing 100081
China
zhangyi2000@263.net